High sensitivity H₂S gas sensors using lead halide perovskite nanoparticles

Ahmad I. Ayesh [a],[*], S.A. Alghamdi [b], Belal Salah [a], S.H. Bennett [b], C. Crean [b], P.J. Sellin [b]

[a] Physics Program, Department of Math., Stat. and Physics, College of Arts and Sciences, Qatar University, P.O.Box 2713, Doha, Qatar
[b] Department of Physics, University of Surrey, Guildford GU2 7XH, UK

ARTICLE INFO

ABSTRACT

We report the development of a high sensitivity H₂S gas sensor based on perovskite nanoparticles, which can be synthesized using relatively simple solution-growth methods. The gas sensor was fabricated from the metal halide perovskite formamidinium lead bromide (FAPbBr₃), which exhibits a high sensitivity to H₂S gas in the form of changes to the electrical conductivity. The response of the sensor to H₂S gas showed a high sensitivity to gas concentrations in the range 0.5 – 100 ppm, with a fast response time of less than one minute under ambient room conditions.

Introduction

Development of selective and sensitive environmental gas sensors is essential to monitor and control the quality of air in crowded cities [1,2]. Hydrogen sulfide (H₂S) is a life threatening gas when present with concentrations above 100 ppm, and it is generated from natural sources such as sulfate-reducing of hydrocarbons and through separation of sour gas [3,4]. However, it is mainly produced through functions related to petroleum extraction and refining [5,6]. Conductometric sensors of toxic gases are practical devices for the detection of gas content in an environment through variation of their electrical resistance [7-9]. These types of sensors exhibit numerous advantages such as their simple production procedure, small size, direct reading, and fast response [10,11]. Implementation of nanomaterials as the sensing elements in these sensors enhances their functionality due to the high concentration of reactive sites, thanks to their great surface to volume ratio [12,13].

In recent years, there has been much development of applications of perovskite materials, eg. with the general formula AMX₃, where 'A' represents either an inorganic or organic cation, 'B' is a metal cation, often Pb, and 'X' is a halide anion [14]. In this work we have used the hybrid organic perovskite formamidinium lead bromide (FAPbBr₃, where FA⁺: CH(NH₂)₂⁺), a material which exhibits exceptional optical luminescence, good charge transport, and a high sensitivity to certain gas molecules. Compared to the similar organic perovskite MAPbBr₃ (where MA⁺ is CH₃NH₃⁺), FAPbBr₃ tends to have improved stability for environmental conditions such as humidity, and is also less affected by structural phase changes [15]. Both MAPbBr₃ and the all-inorganic perovskite CsPbBr₃ have been used for gas sensing applications

typically using their chemically-induced change in resistivity. For example, Zhuang et al [16] reported the use of MAPbBr₃ for acetone and NO₂ detection, achieving a minimum detectable concentration of 20 ppm and 200 ppb, respectively, and Maity et al [17] reported the use of MAPbI₃ (MAPI) as an NH₃ gas sensor achieving sensitivities as low as 1 ppm. There are also extensive reports of the role of oxygen molecules in passivating traps in perovskite materials caused by halide vacancies, and their application as O₂ sensors was reported by Stoeckel et al [18]. The use of the metal halide perovskite MAPI for H₂S gas detection has also been reported by Lee et al [19].

In this work we realized a polycrystalline FAPbBr₃ as an H₂S gas sensor in which the perovskite grains are utilized as the gas sensitive elements and the electrical conductivity of the device is directly affected by the presence of low concentrations of H₂S gas. The FAPbBr₃ perovskite was synthesized using a solution-based process, as reported by Saidaminov et al [20]. The FAPbBr₃ nanoparticles are deposited on glass substrate with pre-fabricated interdigitated electrodes. The fabricated sensors showed a strong response to optical light, with a band edge absorption at 580 nm corresponding to a band gap of 2.13 eV. The performance of the sensors is tested for their sensitivity and time of response, demonstrating a high sensitivity against H₂S, as low as 0.5 ppm, with a fast response time.

Experimental

Materials

Lead(II) bromide (98%), Gamma-butyrolactone (GBL) and N,N-

---

dimethylformamide (DMF) were purchased from Sigma Aldrich. Formamidinium Bromide (FABr, 98%) was purchased from Ossila Ltd, UK. All compounds were used without any further purification.

Synthesis

Small millimeter-sized FAPbBr$_3$ crystals were grown by the Inverse Temperature Crystallization (ITC) technique from a 1 M solution of PbBr$_2$/FABr in DMF:GBL (1:1 v/v) as described in [20].

Sensor fabrication

The FAPbBr$_3$ crystals were crushed into a soft powder and then dispersed in toluene. The dispersion was sonicated until it became homogeneous (~15 min). A drop of the FAPbBr$_3$ dispersion was deposited on a substrate with pre-deposited gold electrodes with an interdigitated structure at 25 ℃ and atmospheric pressure [21]. The electrode separation was $200 \mu m$ for all gas response tests. The fabricated gas sensors were consequently dried at 100 ℃ under a continuous flow of nitrogen at 30 sccm for ~ 30 min to avoid impurities and moister. Each device was connected electrically to the test circuit through wires that were fixed to the device by silver paste.

Characterization

A transmission electron microscope (TEM) of high resolution made by FEI (Tecnai-TF20-G2) was employed to produce high quality images that enabled quantification of grain size as well as their morphology. For this purpose, the FAPbBr$_3$ dispersion was deposited on molybdenum grids and left to dry. X-ray diffraction (XRD) analysis was conducted using an Empyrean XRD diffractometer, and it enabled identification of the composition of FAPbBr$_3$ and the crystal structure. XRD measurements were performed by scanning the diffraction angle (2θ) between $10.0 - 80.0°$ with an accuracy of $0.02°$. Herein, the Cu-K_α emission line ($\lambda = 1.5405 Å$) was utilized to establish XRD analysis. Current-voltage (IV) tests were executed before and after gas sensing tests for every sensor, using a Keithley Instruments voltage source and current meter (model 487). The photosensitivity of the devices was measured using a monochromatic light source produced from a quartz halogen lamp coupled to a grating monochromator.

The gas response of the devices was tested inside a Teflon chamber where each device was fixed on a ceramic stage with an adjustable temperature, monitored by a K-type thermocouple. H$_2$S gas was mixed with air using Bronkhorst mass flow and control units, and then injected into the Teflon chamber while sealed for the gas response investigation [21,22]. Adsorption of H$_2$S gas on nanoparticles causes variation of charges on their surfaces that leads to change of their electrical conduction. Therefore, their gas response electrical signal could be measured using an ammeter integrated within a Keithley Instruments

source measurement unit (SMU - model 238) [23]. The gas response was measured at room temperature by observing the resistance change at a fixed voltage of 10.0 V for each device. The gas response of a sensor was defined as $\left| \frac{R_{H2S} - R_{air}}{R_{air}} \right| \times 100$, where R_{H2S} and R_{air} were the device resistances during exposure to either H$_2$S or air, respectively [24]. Here, the local value of the resistance was evaluated by dividing the voltage by the electrical current.

Results and discussion

An image of the typical millimeter-size FAPbB$_3$ crystals prior to crushing is shown in Fig. 1(a). The grain size and morphology of the synthesized FAPbBr$_3$ grains are characterized by TEM as shown in Fig. 1 (b). The figure reveals grains of nanometer size that are semicircular with an average size of $23 \pm 8 nm$. The composition of FAPbBr$_3$ is illustrated by XRD as presented in Fig. 1(c). The figure shows Miller indices of FAPbBr$_3$ that confirm the cubic phase of the FAPbBr$_3$ [25]. The figure is further used to estimate the size of nanoparticles ($2R$) using the (002) peak at a Bragg's angle $2\theta = 29.9°$ by the Scherrer equation [8]:

$$2R = \frac{K\lambda}{\delta \cos\theta} \tag{1}$$

Where K represents a dimensionless shape factor (~0.9) [4], λ is the XRD wavelength, and δ is the XRD full width at half maximum, and θ represents the. The estimated size of nanoparticles is $21.1 \mp 2.1 nm$ which agrees with average size estimated from the TEM image.

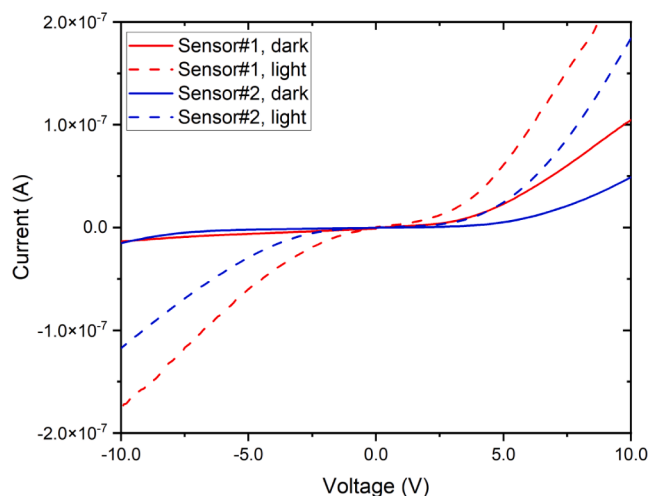Fig. 2 shows the current–voltage characteristics of two FAPbBr$_3$

Fig. 2. Current voltage characteristics of two FAPbBr$_3$ sensors, acquired in the dark and also under semi-light room conditions.
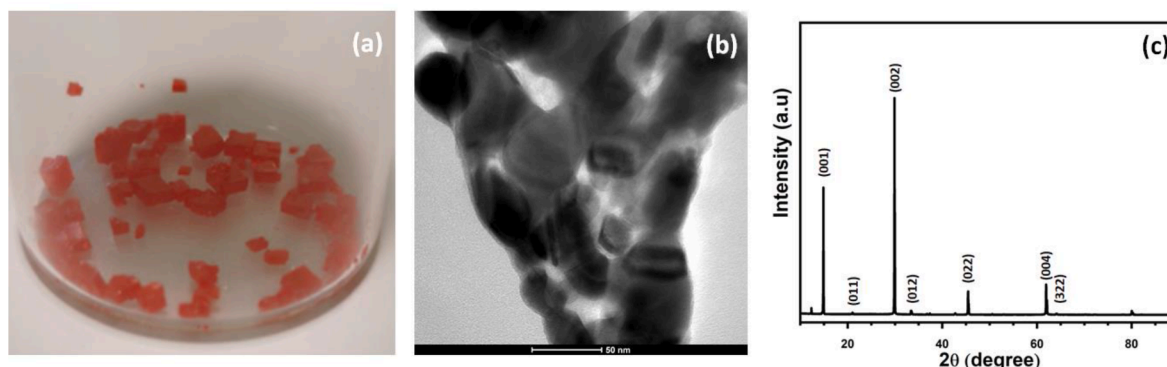
Fig. 1. (a) Picture of the synthesized FAPbBr$_3$ grains. (b) TEM image of the crushed FAPbBr$_3$ grains. (c) XRD spectrum of FAPbBr$_3$ with Miller indices on the figure.

sensors, with the voltage scanned from −10 V to + 10 V. The dark current data shows some asymmetry between positive and negative voltages, with dark current values at −5V of −6nA and −2nA for sensors Q1 and Q2, respectively. When illuminated with 'semi-light' ambient room lighting the photocurrent showed a significant increase due to light, with illuminated current values of at −5V of −60nA and −29nA for sensors Q1 and Q2, respectively. The higher current values of the semi-light measurements as compared with the dark measurements is assigned to absorption of incident radiation that produce electron–hole pairs due to photoexcitation. The applied electric field serves to effectively separate photocarriers and generation of higher electrical current as compared with the dark status. The effect of humidity is tested and minimal effect is observed, i.e the current decreases only by $1 \times 10^{-9} A$ at 5.0V when the humidity is increased from 30% to 45%.

Fig. 3 shows the optical photocurrent measured from one FAPbBr$_3$ sensor as a function of wavelength, acquired at various bias voltages. The photocurrent response shows a sharp decrease at a wavelength of 580 nm, corresponding to the material bandgap at an energy of 2.13 eV. This is consistent with the expected bandgap energy of FAPbBr$_3$, which is strongly dependent on the choice of the halide ion, eg Cl, Br, or I [20].

Fig. 4(a) shows the sensor gas response against H$_2$S gas at selected concentrations performed at room temperature (~25 ºC). The sensor is sensitive at low concentration with a limit of detection (LOD) as low as 0.5 ppm. This value is estimated from the lowest detected value of the response. It should be noted that in case that the response is a linear function of gas concentration, LOD can be calculated as: $(signal − noise ratio) \times \frac{Root mean square of noise}{Slop of linear fitting of responce}$ [26]. The gas response measurements are performed under semi-light conditions (under the normal light of the room at noon time) inside the Teflon chamber, which is semi-transparent to light. Since FAPbBr$_3$ is sensitive to light, the gas response test is repeated under dark conditions as shown in Fig. 4(b). The sensor exhibits a similar trend in response to H$_2$S gas concentration to that achieved under semi-light light, although the response signal is lower (the only change of the response is in the intensity upon exposure to light). Therefore, it can be concluded that the response to H$_2$S is independent on light wavelength. Furthermore, few sensors were tested for their sensitivity against hydrogen gas, but no response. Exposure of FAPbBr$_3$ to light excites free electrons that enhances electrical conduction and the gas response signal. It should be noted that the fabricated devices are highly sensitive at 25 ºC, thus, those devices have low power
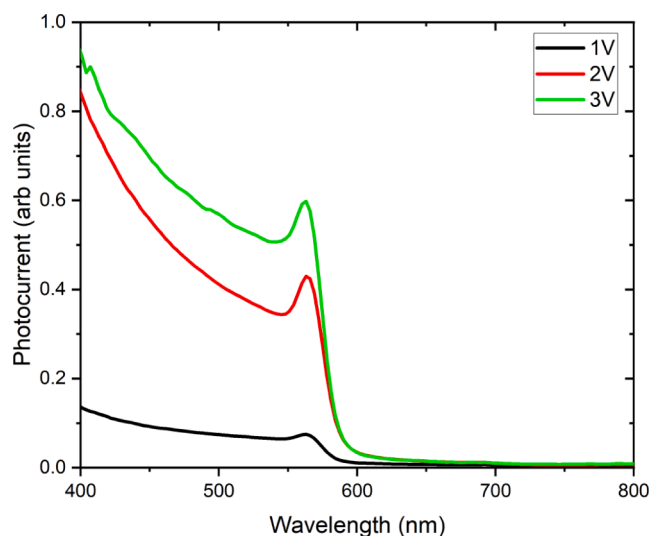
demand since heating of the sensor is not required [6,22,24,27,28]. In addition, there is no need to perform the gas response test at higher temperatures since the response is sufficiently high at low H$_2$S concentrations.

The present sensors exhibit decent performance when compared with recently reported H$_2$S sensors based on perovskites. The nanometer size of FAPbBr$_3$ grains makes them more effective for gas sensing applications, compared to the grains with micro and macro sizes, because of their high ratio of surface to volume [33]. High surface area enables a greater number of reactive sites for adsorption of H$_2$S gas [34]. In general the H$_2$S gas response in a nano-structured semiconductor is due to the adsorption of oxygen ions (for example O$^{2−}$) on the surface of nanoparticles throughout the exposure [6,35]. By this mechanism free electrons are introduced due to adsorption of oxygen ions according to the equation [36]:

$$H_2S + 3O^{2-}(ads) \rightarrow H_2O + SO_2 + 6e^- \tag{2}$$
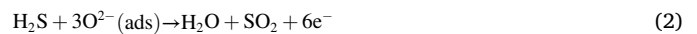
The higher the gas concentration, the higher the generation of SO$_2$ on FAPbBr$_3$ grains, which limits the adoption of additional H$_2$S molecules hence the response drops at fixed H$_2$S concentrations. Furthermore, water vapor may be adsorbed on the surface of FAPbBr$_3$ grains, and then react with H$_2$S gas to produce further electrons and increases the response according to the equations:

$$H_2S + H_2O \leftrightarrow H_2S(aq) \tag{3}$$

$$H_2S(aq) \leftrightarrow HS^- + H^+ \tag{4}$$

$$HS^- \leftrightarrow S^{-2} + H^+ \tag{5}$$
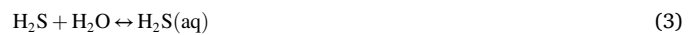
The H$_2$S sensitivity of organic hybrid perovskites has been reported by Lee et al [19] in MAPI, in which the material's sensing mechanism was found to be strongly associated with the presence of both air and moisture. Whilst the exact reaction mechanism in perovskite materials is not yet known, our results are consistent with oxygen molecules increasing the H$_2$S sensitivity.

Upon pausing the flow of H$_2$S gas, the chamber is '*flushed*' by the continuous flow of air thus the generation of new free electrons is stopped. The response signal returns back to its original value, hence, the gas sensing using the FAPbBr$_3$ based sensors is a reversible process (see Fig. 6 (a) below), and those sensors are reusable for multiple operation cycles. This mechanism can be supported by the I(V) characterization which was carried out during and post exposure to H$_2$S gas as presented in Fig. 5. The figure demonstrates that the post exposure I (V) characteristics have lower conductance as compared to that during exposure due to the suspension of generation of free electrons as explained above. The figure shows the nonlinear I(V) characteristics that are considered typical for devices based on percolating granular systems. The effect of humidity of the sensor is tested, and found to have minimal effect on the I(V) characteristics (supplementary figure S1).

Gas sensor stability is a key test to determine the usability of a gas sensor for multiple operation cycles. The fabricated sensors are tested for their stability and reversibility for 10 cycles against 10 ppm at 25 ºC as illustrated in Fig. 6 (a). The figure reveals a reproducible and stable response which supports the usability of the presented sensor. Fig. 6(b) illustrates the response time of the sensors as a function of H$_2$S concentration for both semi-light and dark cases. The figure shows that similar response times are recorded regardless of whether the test is performed under dark or semi-light condition. Furthermore, the response time decreases with increasing H$_2$S concentration, with a maximum value of 1.0 min and minimum of 0.2 min. The figure also shows the recovery time of the produced sensors as a function of H$_2$S concentration for both semi-light and dark cases. The figure demonstrates that the recovery time is almost constant at different H$_2$S concentrations, with average values of 1.6 min for the case of semi-light and 1.4 min for the case of dark. The lower recovery time for the dark case might be due to the lower concentration of photo-generated free
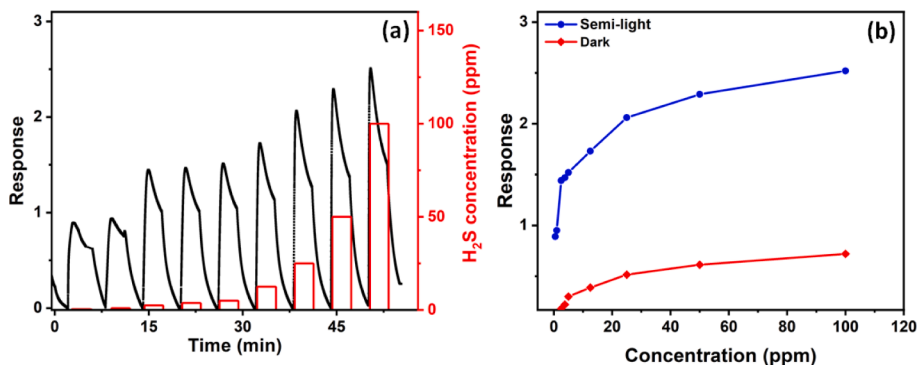

Fig. 3. Optical photocurrent measured from one FAPbBr3 sensor as a function of wavelength, acquired under three bias conditions of 1 V, 2 V and 3 V. The photocurrent response edge at 580 nm corresponds to the material bandgap at 2.13 eV.

Fig. 4. (a) Sensor gas response at different gas concentration while the sensor is inside the Teflon chamber and room light is on. (b) Electrical gas response of the sensor as a function of H_2S concentration while room light is on and the dark measurements.
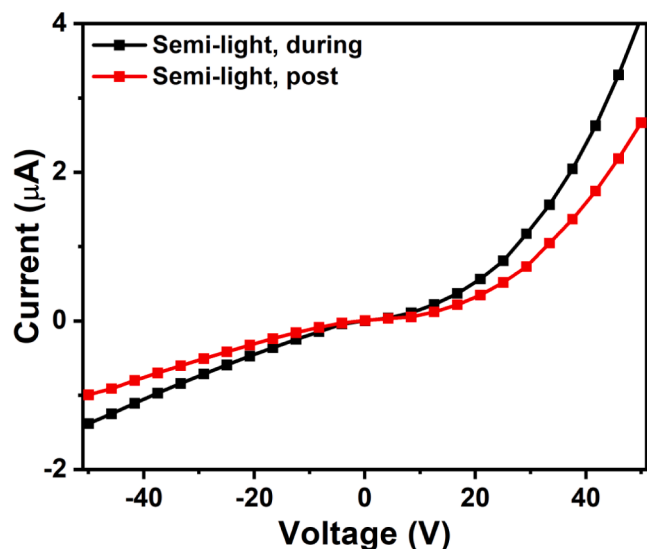

Fig. 5. I(V) characterization of FAPbBr$_3$ based sensors during and post exposure to H_2S gas.

electrons. Nevertheless, the response time is a more important factor for the sensor when it comes to safety applications [37]. Table 1. shows a comparison of the the performance of the present sensor with recently reported ones. Accordingly, the fabricated sensors exhibit an improved response time as compared with the reported values of similar systems for H_2S sensors [28].

Conclusion

High sensitivity conductometric H_2S gas sensors were fabricated based on perovskite nanoparticles of metal halide perovskite formamidinium lead bromide (FAPbBr$_3$). The nanoparticles were synthesized by a solution-growth method. The nanoparticles had an average size of 23 ± 8 nm and cubic structure. Photocurrent measurements revealed that the bandgap of FAPbBr$_3$ is 2.13 eV. The sensors demonstrated high sensitivity toward H_2S, as low as 0.5 ppm under ambient room conditions. The sensors were functional at both dark and semi-light conditions with higher response at semi-light since the nanoparticles are photosensitive. Furthermore, they are stable for multiple test cycles with a minimum response and recovery times of 0.2 min and 0.6 min, respectively, and they have low power demand since heating of the sensor is not required. Accordingly, they can be considered as potential candidates for prototype applications.

CRediT authorship contribution statement

Ahmad I. Ayesh: Conceptualization, Methodology, Formal analysis,

Table 1
Response of recently reported H_2S sensors based on perovskites.

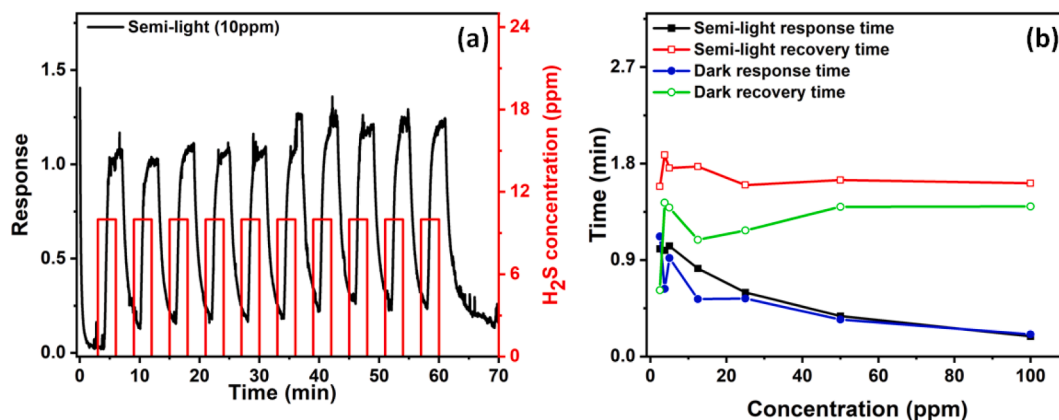| Material	Response	Temperature (°C)	Reference
FAPbBr$_3$	0.5	25	Current work
hexagonal YMnO$_3$	20	100	[29]
NbWO$_6$	0.5	150	[30]
ZnO- La$_{0.8}$Sr$_{0.2}$FeO$_3$	4	200	[31]
Pd-La$_{0.7}$Pb$_{0.3}$Fe$_{0.4}$Ni$_{0.6}$O$_3$	150	200	[32]

Fig. 6. (a) Gas response stability test at 10 ppm of H_2S performed at room temperatures. (b) Response and recovery times of the sensor for both semi-light and dark cases.

Declaration of Competing Interest

The authors declare that they have no known competing financial interests or personal relationships that could have appeared to influence the work reported in this paper.

Acknowledgment

Appendix A. Supplementary data

Supplementary data to this article can be found online at https://doi.org/10.1016/j.rinp.2022.105333.

References

[1] Ayesh AI. Effect of CuOx additive site to graphene nanoribbon on its adsorption for hydrogen sulfide. Results Phys 2021;24:104199.

[2] Kortidis I, Swart HC, Ray SS, Motaung DE. Detailed understanding on the relation of various pH and synthesis reaction times towards a prominent low temperature H2S gas sensor based on ZnO nanoplatelets. Results Phys 2019;12:2189–201.

[3] Wang R. Physiological implications of hydrogen sulfide: a whiff exploration that blossomed. Physiol Rev 2012;92:791–896.

[4] Haija MA, Abu-Hani AFS, Hamdan N, Stephen S, Ayesh AI. Characterization of H2S gas sensor based on CuFe2O4 nanoparticles. J Alloy Compd 2017;690:461–8.

[5] Abu-Hani AFS, Awwad F, Greish YE, Ayesh AI, Mahmoud ST. Design, fabrication, and characterization of low-power gas sensors based on organic-inorganic nanocomposite. Org Electron 2017;42:284–92.

[6] Ayesh AI, Abu-Hani AFS, Mahmoud ST, Haik Y. Selective H2S sensor based on CuO nanoparticles embedded in organic membranes. Sens Actuators, B 2016;231: 593–600.

[7] Ayesh AI. Metal/metal-oxide nanoclusters for gas sensor applications. Journal of Nanomaterials 2016;2016:1–17.

[8] Ayesh AI, Haija MA, Shaheen A, Banat F. Spinel ferrite nanoparticles for H2S gas sensor. Appl Phys A 2017;123:682.

[9] Ayesh AI. Linear hydrogen gas sensors based on bimetallic nanoclusters. J Alloy Compd 2016;689:1–5.

[10] Rosenberg M, Kulkarni G, Bosy A, McCulloch C. Reproducibility and sensitivity of oral malodor measurements with a portable sulphide monitor. J Dent Res 1991;70: 1436–40.

[11] Moradi Z, Fallah H, Hajimahmoodzadeh M. Nanocomposite perovskite based optical sensor with broadband absorption spectrum. Sens Actuators, A 2018;280: 47–51.

[12] Comini E, Faglia G, Sberveglieri G, Pan Z, Wang ZL. Stable and highly sensitive gas sensors based on semiconducting oxide nanobelts. Appl Phys Lett 2002;81: 1869–71.

[13] Gaidi M. Nanostructured SnO 2 thin films: effects of porosity and catalytic metals on gas-sensing sensitivity. Appl Phys A 2018;124:725.

[14] Bibi I, Nazeer Z, Majid F, Ata S, Hakami O, Talib I, et al. Structural, electrochemical and photocatalytic properties of zinc doped Co1-xZn1. 5xFeO3 perovskites prepared by auto combustion sol–gel approach. Results Phys 2021;26:104392.

[15] Zhu Z, Sun Q, Zhang Z, Dai J, Xing G, Li S, et al. Metal halide perovskites: stability and sensing-ability. J Mater Chem C 2018;6(38):10121–37.

[16] Zhuang Y, Yuan W, Qian L, Chen S, Shi G. High-performance gas sensors based on a thiocyanate ion-doped organometal halide perovskite. PCCP 2017;19(20): 12876–81.

[17] Maity A, Raychaudhuri A, Ghosh B. High sensitivity NH 3 gas sensor with electrical readout made on paper with perovskite halide as sensor material. Sci Rep 2019;9: 1–10.

[18] Stoeckel M-A, Gobbi M, Bonacchi S, Liscio F, Ferlauto L, Orgiu E, et al. Reversible, fast, and wide-range oxygen sensor based on nanostructured organometal halide perovskite. Adv Mater 2017;29(38):1702469. https://doi.org/10.1002/adma.201702469.

[19] Lee K-Y, Hsieh J-C, Chen C-A, Chen W-L, Meng H-F, Lu C-J, et al. Ultrasensitive detection of hydrogen sulfide gas based on perovskite vertical channel chemosensor. Sens Actuators, B 2021;326:128988. https://doi.org/10.1016/j.snb.2020.128988.

[20] Saidaminov MI, Abdelhady AL, Maculan G, Bakr OM. Retrograde solubility of formamidinium and methylammonium lead halide perovskites enabling rapid single crystal growth. Chem Commun 2015;51(100):17658–61.

[21] Ayesh AI, Alyafei AA, Anjum RS, Mohamed RM, Abuharb MB, Salah B, et al. Production of sensitive gas sensors using CuO/SnO 2 nanoparticles. Appl Phys A 2019;125:550.

[22] Haija MA, Chamakh M, Othman I, Banat F, Ayesh AI. Fabrication of H 2 S gas sensors using Zn x Cu 1–x Fe 2 O 4 nanoparticles. Appl Phys A 2020;126:1–9.

[23] Ayesh AI, Salah B, Nawwas R, Alyafei A, AlMansouri S, Al-Sulaiti L. Production of flexible nanocomposite membranes for x-ray detectors. Appl Surf Sci 2020;528: 146958.

[24] Haija MA, Ayesh AI, Ahmed S, Katsiotis MS. Selective hydrogen gas sensor using CuFe2O4 nanoparticle based thin film. Appl Surf Sci 2016;369:443–7.

[25] Zhang Y, Yang B, Zheng K, Yang S, Li Y, Deng W, et al. Formamidinium Lead Bromide (FAPbBr 3) Perovskite Microcrystals for Sensitive and Fast Photodetectors. Nano-Micro Letters 2018;10:43.

[26] Ma D, Su Y, Tian T, Yin H, Zou C, Huo T, et al. Multichannel Room-Temperature Gas Sensors Based on Magnetic-Field-Aligned 3D Fe3O4@SiO2@Reduced Graphene Oxide Spheres. ACS Appl Mater Interfaces 2020;12:37418–26.

[27] Salih E, Ayesh AI. DFT investigation of H2S adsorption on graphenenanosheets and nanoribbons: Comparative study. Superlattices Microstruct 2020;146:106650. https://doi.org/10.1016/j.spmi.2020.106650.

[28] Salih E, Ayesh AI. Computational study of metal doped graphene nanoribbon as a potential platform for detection of H2S, Materials Today. Communications 2021; 26:101823. https://doi.org/10.1016/j.mtcomm.2020.101823.

[29] Balamurugan C, Lee DW. Perovskite hexagonal YMnO3 nanopowder as p-type semiconductor gas sensor for H2S detection. Sens Actuators, B 2015;221:857–66.

[30] Wang J, Ren Y, Liu H, Li Z, Liu X, Deng Y, et al. Ultrathin 2D NbWO6 Perovskite Semiconductor Based Gas Sensors with Ultrahigh Selectivity under Low Working Temperature. Adv Mater 2022;34(2):2104958. https://doi.org/10.1002/adma.v34.210.1002/adma.202104958.

[31] Syue Y-K, Hsu K-C, Fang T-H, Lee C-I, Shih C-J. Characteristics and gas sensor applications of ZnO-Perovskite heterostructure. Ceram Int 2022. https://doi.org/10.1016/j.ceramint.2022.01.126.

[32] S. Jagtap, A. Kadu, V. Sangawar, S. Manorama, G. Chaudhari, H2S sensing characteristics of La0. 7Pb0. 3Fe0. 4Ni0. 6O3 based nanocrystalline thick film gas sensor, Sensors and Actuators B: Chemical, 131 (2008) 290-294.

[33] Shipway AN, Katz E, Willner I. Nanoparticle arrays on surfaces for electronic, optical, and sensor applications. ChemPhysChem 2000;1(1):18–52.

[34] Frey GL, Tenne R, Matthews MJ, Dresselhaus M, Dresselhaus G. Raman and resonance Raman investigation of MoS 2 nanoparticles. Physical Review B 1999; 60:2883.

[35] Ayesh AI, Ahmed RE, Al-Rashid MA, Alarrouqi RA, Saleh B, Abdulrehman T, et al. Selective gas sensors using graphene and CuO nanorods. Sens Actuators, A 2018; 283:107–12.

[36] Haija MA, Basina G, Banat F, Ayesh AI. Adsorption and gas sensing properties of CuFe2O4 nanoparticles. Materials Science-Poland 2019;37:289–95.

[37] Zhu L, Zeng W. Room-temperature gas sensing of ZnO-based gas sensor: A review. Sens Actuators, A 2017;267:242–61.